

# Analysis of Furnace Operational Parameters for Controllable Annealing of Thin Films

Victor Ovchinnikov

Department of Aalto Nanofab  
School of Electrical Engineering, Aalto University  
Espoo, Finland  
e-mail: Victor.Ovchinnikov@aalto.fi

**Abstract**—Annealing of thin silver films in different furnaces is studied. It is shown that identical parameters of thermal treatment do not guarantee reproducibility and annealing provides different results, e.g., shape and size of nanostructures, in different furnaces. To clarify the source of variation, morphology and reflectance spectra of the samples are analyzed. Additionally, numerical simulation of heating process in a diffusion furnace has been performed. It is demonstrated that uncontrollable heating and cooling of silver film itself leads to variation of annealing results.

**Keywords**—self-assembling; silver thin film; diffusion furnace; annealing

## I. INTRODUCTION

Annealing is well known and broadly used in microfabrication heat treatment of inorganic materials. In case of polymer, heat treatment is called baking, curing or drying. From the beginning of semiconductor technology, annealing is used to modify properties of thin films, substrates and interfaces. Annealing is not the crucial microfabrication method like lithography or etching, but it is utilized in every process flow for doping of semiconductors, silicide formation, densification of deposited films and sample surface conditioning [1]. Annealing is done in furnaces, which can have different design: convection and diffusion furnaces, hot plates and rapid thermal processing tools, infrared (IR) and curing ovens. Usual description of annealing in publications includes only temperature and duration of the process [1, 2]. Sometimes information about gas flow is added [3, 4] and it is very seldom written about furnace design and sample position in the furnace [5]. However, different annealing tools deliver heat energy to a sample in different ways what directly affects on obtained results.

During annealing, the heat exchange between sample and furnace is performed by thermal conductivity, convection and thermal radiation. Depending on furnace design, one or other heat transfer mode can be done dominant. For example, a hot plate mainly heats a sample by thermal conductivity, a diffusion furnace - by thermal radiation and convection, an IR oven - by thermal radiation. In all furnaces heat is not only generated, but is also dissipated. As a result, the sample temperature is controlled by thermal balance between heating and cooling processes.

Additionally, the sample thermal parameters (emissivity, thermal conductivity and heat capacitance) and sample arrangement in a furnace (position, holder design and shields) affect on the heating process dynamics and the sample temperature. The most complicate situation happens in case of phase transition of the heated thin film, e.g., melting or recrystallization. As a consequence, the sample emissivity is changed and the new thermal balance is installed.

In this paper, we demonstrate that identical heating ramp, temperature and time of the annealing are not sufficient conditions for reproducing of nanostructures fabricated by annealing of thin silver films. We compare design of three annealing tools and analyze relative strength of different heating modes in all tools. On the base of optical properties and crystalline structure of the annealed and as-deposited samples we make conclusions about melting and crystallization of silver nanostructures. To find temperature field of the furnace and the real sample temperature we simulate the heating processes in the diffusion furnace for different gas flows and sample emissivities. The obtained results are used to find correlation between annealing conditions and morphology of silver nanostructures.

The paper is organized as follows. In the subsequent Section II, details of sample preparation and measurement procedures are presented. In Section III, the results of work are demonstrated by scanning electron microscope (SEM) images and reflectance spectra of the silver films and also by heat transfer simulations. The effect of furnace design on silver film annealing is discussed in Section IV. In Section V, the conclusions are drawn.

## II. EXPERIMENTS

Four identical samples were prepared to compare annealing in different furnaces. For this purpose, a 12 nm thick silver film was deposited by electron beam evaporation at rate 0.2 nm/s. As a substrate was used 4" silicon wafer with 21 nm layer of thermal oxide. After deposition the whole wafer was cut on four quotes, which were further processed separately. Annealing was done at 400 °C during 5 minutes with heating ramp 21 °C/min, and cooling ramp 3.6 °C/min. However, all samples were processed in various furnaces (Fig. 1).

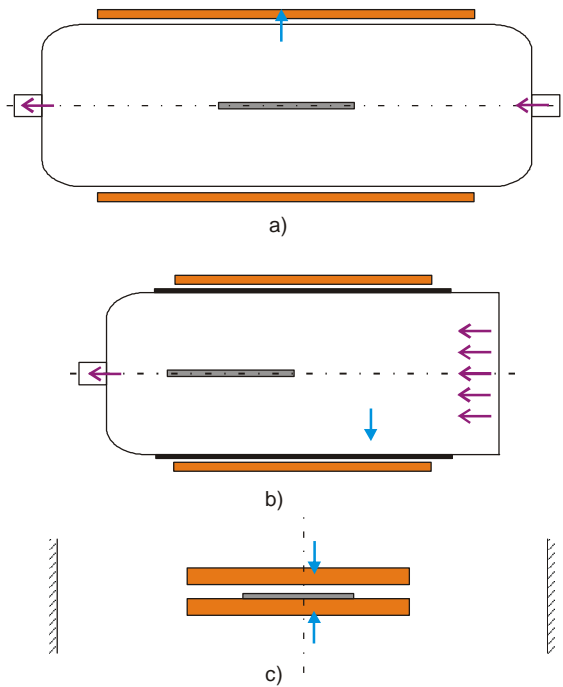


Figure 1. Design of the diffusion furnace (a), the fast ramping furnace (b) and the hot plate (c). Thermocouple positions and gas flows are denoted by blue and violet arrows, respectively. Heating surfaces are orange.

The sample #1 was annealed in the diffusion furnace (Fig. 1a). As a sample holder was used a 4" silicon wafer on a quartz boat, which was located in the centre of the furnace during experiment. It was supposed that heat exchange through the quartz boat was negligible. The quartz furnace

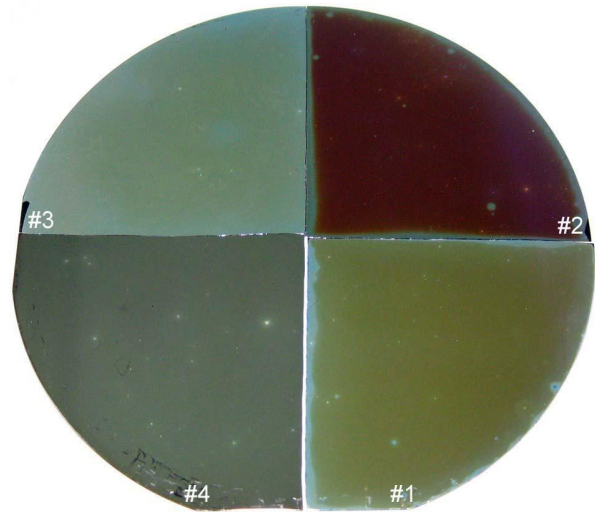


Figure 2. Optical images of the annealed (#1 - #3) and as-deposited (#4) samples.

tube had 4½ inch diameter, 96 cm length and 3 mm thick walls. The resistive heater (orange strips in Fig. 1a) was situated around the tube with the gap 1 cm. The furnace temperature was controlled according to thermocouple measurements on the tube surface. Room temperature nitrogen with flow  $8.3 \times 10^{-5}$  standard  $m^3/s$  was introduced in the furnace along its axis.

The sample #2 was annealed in a fast ramping furnace (Fig. 1b). Temperature, gas flow and process duration were similar for both furnaces (Fig. 1a and 1b). However, in the

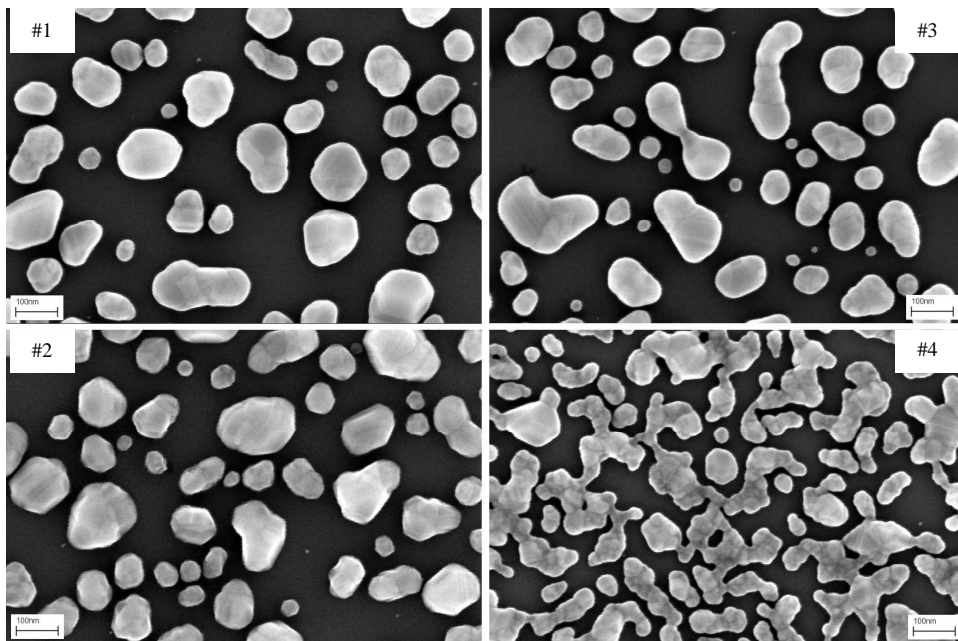


Figure 3. Plan SEM images of the annealed (#1 - #3) and as-deposited (#4) samples.

fast ramping furnace the quartz tube length was 35 cm and the sample position was close to the exhaust of furnace. As a heater were used tungsten lamps. The quartz tube was covered by the heat absorbing shield (black lines in Fig. 1b). The gas temperature in the tube was measured by thermocouple and was used for process control. Nitrogen was introduced through array of holes in the right part of the furnaces. The sample #3 was annealed between two hot plates in vacuum (Fig. 1c). Both hot plates had 4 inch in diameter and were separated by 2.5 mm gap. The chamber wall temperature was close to room temperature.

The silver films were deposited in the e-beam evaporation system IM-9912 (Instrumenti Mattila Oy) at base pressure of  $2.7 \times 10^{-5}$  Pa and at room temperature of the substrate. Annealing of the sample #1 was done in the diffusion furnace THERMCO Mini Brute MB-71. Annealing of the sample #2 was done in the fast ramping furnace PEO-601 from ATV Technology GmbH. Annealing of the sample #3 was done in the wafer bonder AML AWB-04 from Microengineering Ltd.

Plan view SEM images of the samples were observed with the Zeiss Supra 40 field emission scanning electron microscope. Reflectance measurements were carried out using the FilmTek 4000 reflectometer in the spectral range from 400 to 1700 nm. Crystalline structure of the silver films was estimated by reflection high-energy electron diffraction (RHEED) observations with the help of the diffractometer embedded in a molecular beam epitaxy tool.

### III. RESULTS

Fig. 2 shows the optical image of three annealed samples (#1-#3) and as-deposited silver film (#4). The picture was taken by the digital camera with flash. Despite of identical temperature and time of annealing all samples have different colours of surface. The sample #1 is yellow-green, the sample #2 is brown-red, the sample #3 is yellow-blue and the as-deposited sample is grey. Bulk silver is a perfect reflector, however, nanostructured silver possesses plasmon resonances, which modify reflection spectra of the samples [5-7]. Therefore, the obtained colour variation could be explained by silver nanostructures formed on the sample surface instead of the continuous silver film. To clarify the suggestion we have observed all samples in SEM (Fig. 3). The as-deposited silver film (#4) is already discontinuous, has lace like structure and silver covers relatively large part of surface in comparison with annealed films. The annealed samples have close values of silver areal density and nanostructure sizes, but shape of nanoislands depends on annealing conditions. The sample #2 demonstrates most irregular islands with straight flats on some of them. The sample #3 has roundish nanostructures with large shape deviation and the sample #1 shows intermediate picture between two previous cases. The height of all annealed nanostructures is around 30 nm.

It was mentioned above that colour variation of the samples could be explained by their reflection spectra, which are connected with plasmonic properties of nanostructures. Fig. 4a demonstrates reflection spectra of the annealed and

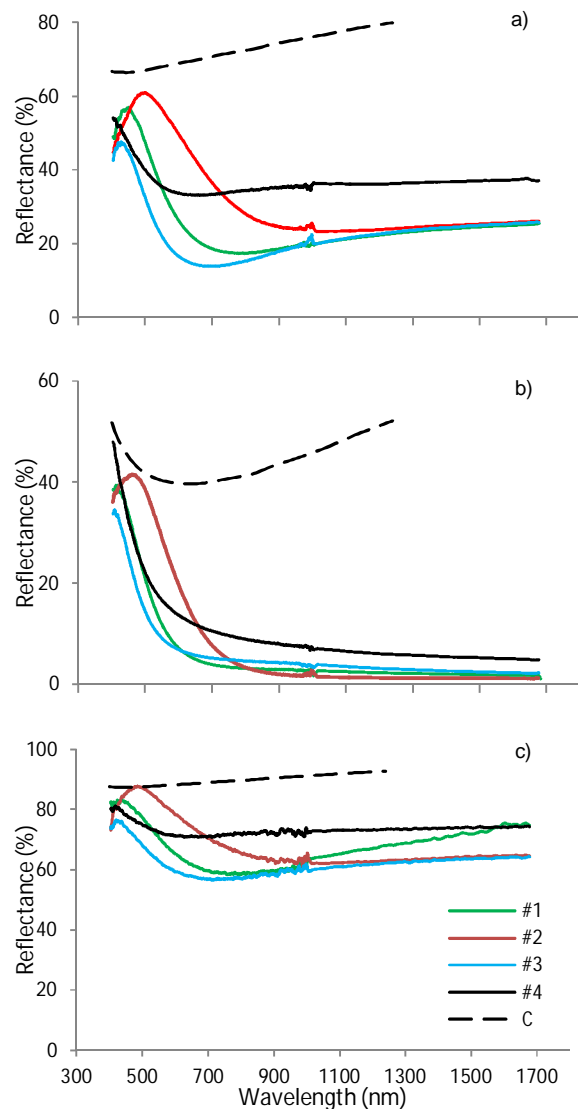


Figure 4. Reflection spectra for normal (a) and inclined ( $70^\circ$ ) light incident for *p*- (b) and *s*- polarization (c). Dashed lines show calculated spectra.

as-deposited samples at normal light incidence. In the Fig. 4b and 4c the same spectra are shown for inclined light incident ( $70^\circ$ ) and for *p*- and *s*- polarization, respectively. According to surface colour, the sample #2 has main peak at the longest wavelength 498 nm, the sample #3 at the shortest wavelength 411 nm and the sample #1 at the intermediate wavelength 449 nm for *s*-polarized light (Fig. 4c). The as-deposited sample (#4) has no reflection peaks in the range of measurements, but it has trough at the wavelength 658 nm.

On the other hand, the sample #2 has no troughs at all and the samples #3 and #1 have troughs at 694 nm and 806 nm, respectively. For *p*-polarized light strong reflection is observed only in visible range (below 800 nm). In IR

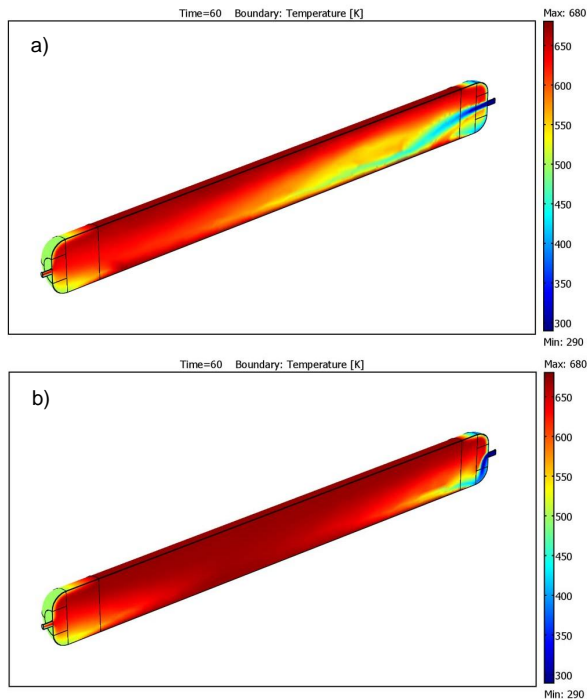


Figure 5. Temperature fields of the diffusion furnace for high (a) and low (b) nitrogen flows. The gas inlet is on the right.

$p$ -polarized reflectance falls down to 1-2% for all annealed samples and to 5% for the as-deposited sample. In IR range (above 1200 nm), spectra of the annealed samples coincide with each other what justifies suggestion about identical silver areal density. Dashed lines show theoretical spectra of the samples, calculated with the help of bulk silver optical parameters.

The RHEED showed relatively sharp, continuous Laue circles in addition to amorphous background pattern for the sample #3. Therefore, this sample contains separate crystalline particles, but their orientation varies from island to island [8]. For other samples, intensity and sharpness of the diffraction patterns were weaker and decreased in the following order: sample #1, as-deposited sample, sample #2. In other words, sample #2 includes nanoislands with the most disordered crystalline structure.

3D simulations of annealing process were done for the diffusion furnace (Fig. 1a) with the help of software COMSOL Multiphysics 3.5a. Due to high computational load the simulations were done in two phases. Firstly, temperature and velocity fields inside of the empty furnace were found. For this purpose two models were used in coupled mode: general heat transfer model (calculates thermal conduction and convection) and Navier –Stokes model for non-isothermal flow. Gravitational force arisen due to gas density variation was taken into account in the Navier –Stokes model. At the second phase, the obtained temperature and velocity of gas were used as boundary conditions for simulation of silicon wafer heating in the hot cylindrical tube. At this stage all heat transfer modes, including sample, tube and gas thermal conduction,

convection in nitrogen and surface-to-surface radiation were taken into account.

Fig. 5 demonstrates the simulation results obtained at the first phase. Temperature distributions in the diffusion furnace (Fig. 1a) were calculated for quartz tube temperature 400 °C and for gas flows  $8.3 \times 10^{-5}$  standard  $m^3/s$  (Fig. 5a) and  $1.0 \times 10^{-5}$  standard  $m^3/s$  (Fig. 5b). Large flow of cold gas creates non-uniform temperature distribution inside of the tube and the gas temperature in the middle of the furnace (below sample holder) can be 150 °C lower than the tube temperature (Fig. 5a). At the same place gas velocity reaches maximum value 0.18 m/s. At small flow of nitrogen (Fig. 5b), temperature variation and gas velocity in the middle of furnace do not exceed 15 °C and 0.03 m/s, respectively.

Temperature and velocity fields near the wafer are illustrated in Fig. 6a and Fig. 6b, respectively. They are obtained at the second phase of simulations (temperature and velocity of gas at the entrance are taken from Fig. 5a) for nitrogen flow  $8.3 \times 10^{-5}$  standard  $m^3/s$  and sample emissivity  $\varepsilon=1$ . The internal furnace volume is divided by the wafer-holder in two parts – the upper one with high temperature and low velocity and the lower one with low temperature and high velocity. In the upper volume gas has temperature 398 °C and slowly moves with velocity 0.02 m/s. In the lower volume high temperature and velocity gradients exist. However, the wafer temperature variation does not exceed 1°C due to high thermal conductivity of silicon. In the present experiment, the wafer temperature depends on tube

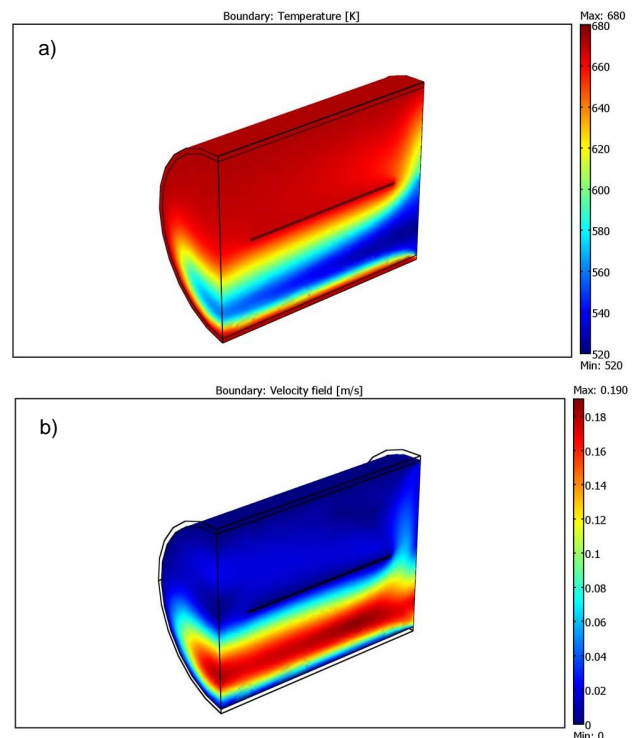


Figure 6. Temperature (a) and velocity (b) fields near the wafer for high nitrogen flow and  $\varepsilon=1$ . Gas moves from right to left.

temperature, nitrogen flow and wafer emissivity  $\epsilon$ . Cross sections of the temperature fields in the centre of the furnace for  $\epsilon=1$  and  $\epsilon=0$  are given in Fig. 7a and Fig. 7b, respectively. Temperature of the heat absorbing sample ( $\epsilon=1$ ) is 35 °C higher than temperature of the reflective sample ( $\epsilon=0$ ). As a consequence, the temperature distribution in the upper volume is more uniform for  $\epsilon=1$ .

#### IV. DISCUSSION

Annealing of thin silver films is complicated by three circumstances. Firstly, silver films and nanostructures are melted at low temperature [3, 9, 10]. In our previous study [5], it was shown that this melting point is close to 250 °C. However, this transformation happens only once and the second heating of the sample does not change morphology of silver nanostructures. Secondly, liquid silver tends to spherical shape of nanoislands due to low cohesive forces to SiO<sub>2</sub> surface. Thirdly, silver is the best plasmonic material [6] and silver nanostructures appeared after breaking apart continuous film modify optical properties of the sample surface [7].

The first sign of not identical annealing conditions in the studied furnaces is different sample colours (Fig. 2) and

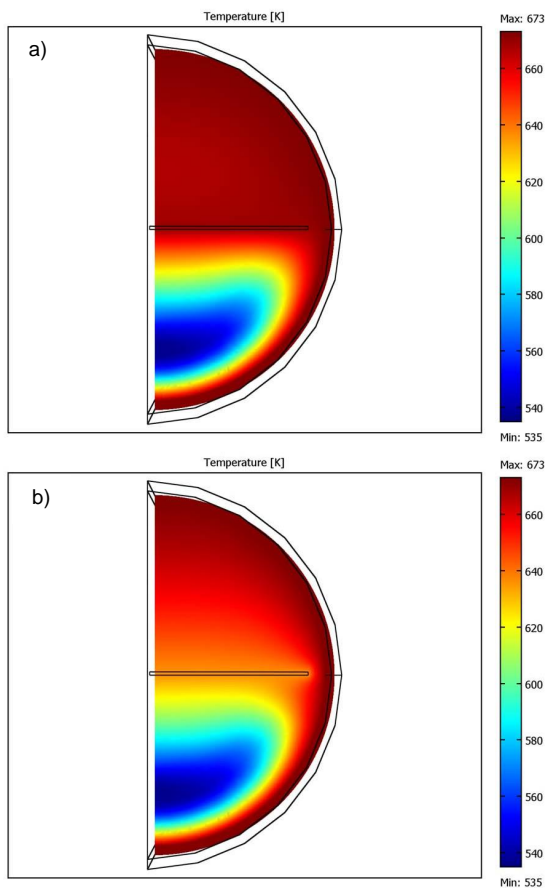


Figure 7. Vertical cross sections of the temperature fields at high nitrogen flow in the centre of the furnace for  $\epsilon=1$  (a) and  $\epsilon=0$  (b).

corresponding changing of reflection spectra after annealing (Fig. 4). Reflection spectra demonstrate strong plasmon properties of silver nanostructures formed after silver film annealing. The troughs in the range 690 – 810 nm correspond to dipole plasmon resonance and peaks at 410 – 500 nm correspond to quadrupole resonance [7]. The non-annealed sample possesses only very weak dipolar plasmon resonance (see spectrum of as-deposited sample). Till some extent plasmon properties can be estimated by the difference between calculated and measured spectra – the larger difference, the stronger plasmon resonances. Based on this criterion, the strongest plasmon resonances are observed in the sample #3. Plasmon properties are very sensitive to asymmetry of dielectric environment. In the studied samples, refractive index of silicon ( $n=3.5$ ) is much higher than refractive index of SiO<sub>2</sub> ( $n=1.5$ ). Due to this local electric field is concentrated in silicon and optical properties of silver are modified. It is illustrated by reflection of  $p$ -polarized light (Fig. 4b), which mainly excites electric field at silver/substrate interface. For  $p$ -polarization deviations of real spectra from calculated ones are much larger than for  $s$ -polarized light.

In Section III, we have shown that that all annealed samples have close values of silver areal density and nanostructure sizes. Therefore, relatively large redshift of peaks and troughs in Fig. 4 cannot be only explained by changing of island geometry. Due to identity of the studied samples, the spectrum variations can be only connected with material modification, e.g., changing of silver dielectric function. Moreover, from spectral peak and trough broadening (the broadest peak has sample #2) follows that imaginary part of silver dielectric function increased [6].

Usually, annealing is used to improve and restore crystalline structure. However, there are reports about increased defect concentration in melted silver samples [11]. Our RHEED observations also showed that crystalline structure of the annealed sample #2 is worse than structure of the as-deposited one. Taking into account the broadest reflection peak and absence of dipolar trough for sample #2 we can conclude that this sample has highest disorder of crystalline structure among the studied samples.

In the diffusion furnace (Fig. 1a) the target temperature 400 °C was supported on the external side of the quartz tube. In the fast ramping furnace (Fig. 1b) the target temperature 400 °C was supported inside of furnace, 1 cm above bottom of the quartz tube. According to Fig. 6a the measured temperature in this point can be 150 °C lower than the tube temperature, i.e., in our experiment the tube temperature of the fast ramping furnace could be close to 550 °C. Nitrogen flow  $8.3 \times 10^{-5}$  standard m<sup>3</sup>/s is very low for the fast ramping furnace (Fig. 1b) and provides laminar gas flow inside tube. In case of diffusion furnace (Fig. 1a), the same nitrogen flow is too high and provides turbulent gas flow in the lower part of the tube (Fig. 5a). Higher temperature of the absorber shield ( $\epsilon=1$ ) around the quartz tube makes thermal radiation in the fast ramping furnace much higher than in the diffusion one.

In case of thin silver layer on silicon, most of radiation energy is absorbed in silver and during heating up in laminar

gas flow (the fast ramping furnace) the silver temperature is higher than the temperature of the substrate. In turbulent gas flow, intensive heat exchange between silver and nitrogen prevents overheating of silver nanostructures (the diffusion furnace).

After melting silver starts to form droplets due to surface tension forces and decreases silver areal density. However, absorbed thermal radiation is proportional to silver areal density or absorbing cross-section. Thus, geometry change decreases radiative heat transfer to silver. The cold substrate cools down silver nanostructures and causes their rapid solidification. The quenching happens without proper crystallization and silver solidifies in amorphous phase (sample #2).

In case of low radiative heat transfer (samples #1, #3), melting happens at higher substrate temperature and without silver overheating. Depending on conductive and radiative heat fluxes the melted silver is cooled with much lower rate and solidifies in polycrystalline phase. In our study, sample #3 has the best crystalline structure due to lower cooling rate between two hot plates in vacuum. One of the reasons for quenching in this case is reduction of the surface energy [12]. Another reason is heating of silver nanostructures by conductive flux through interfacial thermal resistance. Silver melting acquires additional heat flux from the substrate to the nanostructure. This heat flux increases temperature drop on the interfacial thermal resistance between the substrate and the silver droplet, what in turn leads to decreasing of silver temperature and quenching.

## V. CONCLUSIONS

We have demonstrated that annealing of identical samples in identical conditions, but in different furnaces leads to different results. The effect of furnace operational parameters (gas flow, sample and thermocouple position, sample emissivity) on annealing of thin silver films has been analyzed. Radiation heating of silver films can be very strong and provides overheating of the silver relatively substrate. However, silver areal density is shrunk after melting and droplet formation what causes decrease of radiation heating. As a result, melted structures are quenched to solid state with irregular shape and high crystalline disorder. The effect depends on rate of solidification and explains variation of annealing results from furnace to furnace.

## ACKNOWLEDGMENT

This research was undertaken at the Micronova Nanofabrication Centre of Aalto University.

## REFERENCES

- [1] S. Franssila, "Introduction to Microfabrication", 2nd edition, Wiley, 2010, 534p.
- [2] V. Ovchinnikov, A. Malinin, S. Novikov, and C. Tuovinen, "Silicon Nanopillars Formed by Reactive Ion Etching Using a Self-Organized Gold Mask", *Physica Scripta*, vol. T79, 1999, pp. 263-265.
- [3] S. R. Bhattacharyya et al., "Growth and Melting of Silicon Supported Silver Nanocluster Films", *J. Phys. D: Appl. Phys.*, vol. 42, 2009, pp. 035306-1 - 035306-9.
- [4] D. Adams, T. L. Alford, and J. W. Mayer, "Silver Metallization: Stability and Reliability", Springer, 2008, 123p.
- [5] V. Ovchinnikov, "Effect of Thermal Radiation during Annealing on Self-organization of Thin Silver Films", *Proceedings of ICQNM 2013*, ThinkMind Digital Library (ISBN: 978-1-61208-303-2), pp. 1-6.
- [6] M. A. Garcia, "Surface Plasmons in Metallic Nanoparticles: Fundamentals and Applications", *J. Phys. D: Appl. Phys.*, vol. 44, 2011, pp. 283001-1 - 283001-20.
- [7] V. Ovchinnikov and A. Shevchenko, "Self-Organization-Based Fabrication of Stable Noble-Metal Nanostructures on Large-Area Dielectric Substrates", *Journal of Chemistry*, vol. 2013, 2013, Article ID 158431, pp. 1 - 10., <http://dx.doi.org/10.1155/2013/158431>.
- [8] A. Ichimiya and P. I. Cohen, "Reflection High-Energy Electron Diffraction", Cambridge University Press, 2004, 353p.
- [9] O. A. Yeshchenko, I. M. Dmitruk, A. A. Alexeenko, and A. V. Kotko, "Surface Plasmon as a Probe for Melting of Silver Nanoparticles", *Nanotechnology*, vol. 21, 2010, pp. 045203-1 - 045203-6.
- [10] M. Khan, S. Kumar, M. Ahamed, S. Alrokayan, and M. Salhi, "Structural and Thermal Studies of Silver Nanoparticles and Electrical Transport Study of Their Thin Films", *Nanoscale Research Letters*, vol. 6, 2011, pp. 434-1 - 434-8.
- [11] S. A. Little, T. Begou, R. E. Collins, and S. Marsillac, "Optical Detection of Melting Point Depression for Silver Nanoparticles via in situ Real Time Spectroscopic Ellipsometry", *Appl. Phys. Lett.*, vol. 100, 2012, pp. 051107-1 - 051107-4.
- [12] E. P. Kitsyuk, D. G. Gromov, E. N. Redichev, and I. V. Sagunova, "Specifics of Low Temperature Melting and Disintegration into Drops of Silver Thin Films", *Protection of Metals and Physical Chemistry of Surfaces*, vol. 48, 2012, pp. 304-309.